Optically probing the detection mechanism in a molybdenum silicide superconducting nanowire single-photon detector

Misael Caloz, Boris Korzh, Nuala Timoney, Markus Weiss, Stefano Gariglio, Richard J. Warburton, Christian Schönenberger, Jelmer Renema, Hugo Zbinden, and Félix Bussières

---

Optically probing the detection mechanism in a molybdenum silicide superconducting nanowire single-photon detector

Misael Caloz,[1,a)] Boris Korzh,[1] Nuala Timoney,[1] Markus Weiss,[2] Stefano Gariglio,[3] Richard J. Warburton,[2] Christian Schönenberger,[2] Jelmer Renema,[4] Hugo Zbinden,[1] and Félix Bussières[1,b)]

[1]*Group of Applied Physics, University of Geneva, Chemin de Pinchat 22, CH-1211 Geneva 4 Switzerland*
[2]*Department of Physics, University of Basel, Klingelbergstrasse 82, CH-4056 Basel Switzerland*
[3]*Department of Quantum Matter Physics, University of Geneva, 24, Quai Ernest-Ansermet, CH-1211 Geneva 4 Switzerland*
[4]*Clarendon Laboratory, University of Oxford, Parks Road, Oxford OX1 3PU, United Kingdom*

We experimentally investigate the detection mechanism in a meandered molybdenum silicide superconducting nanowire single-photon detector by characterising the detection probability as a function of bias current in the wavelength range of 750–2050 nm. Contrary to some previous observations on niobium nitride or tungsten silicide detectors, we find that the energy-current relation is nonlinear in this range. Furthermore, thanks to the presence of a saturated detection efficiency over the whole range of wavelengths, we precisely quantify the shape of the curves. This allows a detailed study of their features, which are indicative of both Fano fluctuations and position-dependent effects. *Published by AIP Publishing.* [http://dx.doi.org/10.1063/1.4977034]

Superconducting nanowire single-photon detectors (SNSPDs) are a key technology for optical quantum information processing.[1,2] An SNSPD consists of a thin wire of superconducting material biased close to its critical current, which becomes resistive after the absorption of a single photon, leading to a detection through an amplified voltage pulse. Their low dark count rate, fast response time, small jitter, and high efficiency favour their use in various demanding quantum optics applications such as quantum key distribution,[3] quantum networking,[4] device-independent quantum information processing[5] and deep-space optical communication.[6] Notably, SNSPDs can be integrated into photonic circuits,[7,8] and their applications extend beyond quantum optics, including light detection and ranging,[9] integrated circuit testing,[10] and fiber optic sensing.[11]

One recent important advance in the SNSPD field has been the introduction of amorphous superconductors such as tungsten silicide (WSi),[12] molybdenum silicide (MoSi)[13,14] and molybdenum germanium (MoGe).[15] SNSPDs based on these materials currently have the highest reported detection efficiencies (93% for WSi[12]), as well as a higher fabrication yield[16] than devices made of polycrystalline materials such as niobium nitride (NbN),[1] niobium titanium nitride (NbTiN)[17] and tantalum nitride (TaN).[18] MoSi SNSPDs tailored to specific advanced photon counting applications have recently been reported, including integration on an optical waveguide,[19] UV single-photon detection[20] and integrated ion trapping.[21]

One striking difference with polycrystalline materials is that amorphous SNSPDs have a detection efficiency that saturates at bias currents well below the critical current.[22] Despite the extensive studies, the question remains if these differences are due to a fundamentally different detection mechanism.[23] Moreover, understanding the nature of the detection mechanism may ultimately lead to novel SNSPD structures with better performances or SNSPD-inspired devices targeting a broader range of applications.

One of the main techniques for investigating the detection mechanism is measurements of the energy-current relation, i.e., the amount of photon energy required to produce a detection event at constant detection probability. For NbN, the energy-current relation was found to be linear[24] over a large range of energies using quantum detector tomography[25] (QDT), which is evident for the role of a diffuse cloud of quasiparticles in the detection process.[26] Moreover, the position-dependent measurements[27] and external magnetic field-based study[28] highlight the role of vortices in the detection mechanism. In WSi, a linear relation was found over a large range of energies, but with a slight deviation from a linear behaviour at low energies. Other results are, however, contradictory: in separate experiments, the indications of a nonlinear energy-current relation were found for NbN and WSi SNSPDs.[28] In contrast, no extensive studies have been carried out on amorphous MoSi devices.

In this work, we experimentally investigate the detection mechanism in MoSi SNSPDs. We illuminate a 170 nm wide MoSi SNSPD with wavelengths ranging from 750 to 2050 nm. By recording the photon count rate as a function of the bias current and the incident photon energy, we are able to fully characterise the device response. We find that the energy-current relation is nonlinear throughout this wavelength range. Furthermore, we investigate the shape of the count rate curves at different photon energies. We interpret these results as a potential combination of Fano fluctuations and position-dependent effects in the device.

The device is fabricated out of a 5 nm thick film of amorphous $Mo_{0.8}Si_{0.2}$, with a $T_c = 5$ K, which is deposited by co-sputtering with a DC and RF bias on the molybdenum and silicon targets, respectively. The MoSi film is deposited

a)Electronic mail: misael.caloz@unige.ch
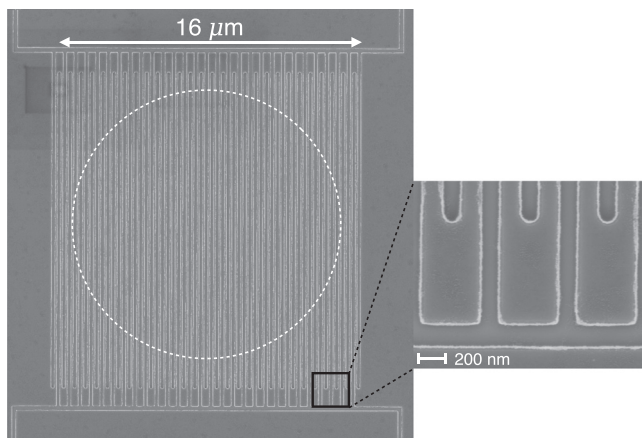b)Electronic mail: felix.bussieres@unige.ch

FIG. 1. Scanning electron microscope image of the MoSi device. The dashed circle shows where the photons are absorbed, corresponding to the limit of the Gaussian mode spread from the optical fiber. The inset on the right shows a magnification of the meander turns.
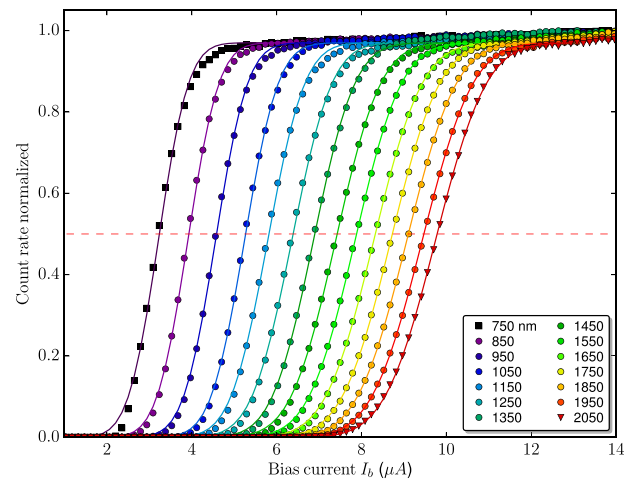

FIG. 2. Normalized photon count rate (detection rate subtracted minus the DCR, normalized by the maximum count rate) as a function of the bias current I_b at 0.75 K. Each colour represents one measurement run with a specific incident photon wavelength. Each solid line traces the error function fit for the respective data curve. The dashed red line indicates the fraction η of the saturated detection efficiency $\eta = 50\%$. The leftmost and rightmost curves correspond to 750 and 2050 nm, respectively. The critical current is 14.7 μA.

on a thermally oxidised silicon wafer and is capped with a 3 nm a-Si layer. The X-ray diffraction measurements have been performed, confirming the amorphous nature of the MoSi. The film is patterned into a meandered wire with a width of 170 nm and a pitch of 160 nm (see Fig. 1) and a total surface area of $16 \times 16 \, \mu m^2$ by a combination of e-beam lithography and ion beam etching. A self-aligning technique is used to ensure optimal coupling to the optical fibre.[29] The detection efficiency at 1550 nm is 20%. The device has been selected out of tens of other detectors with different widths and fill factor by looking for the highest critical current and widest plateau region in order to have the largest energy range accessible. We repeated the experiment with three other devices with similar nanowire widths, and the results obtained were quantitatively the same.

The detector is mounted in a sorption cryostat reaching 0.75 K. The detector is biased with a current source and its critical current is 14.7 μA. The voltage pulses from detection events are amplified by a custom low-noise amplifier cooled to 40 K and by a secondary amplifier at room temperature.

The detector is illuminated with unpolarized photons coming from a halogen lamp sent through a grating monochromator. This provides a continuous spectrum from 750 to 2050 nm. We carefully calibrated the monochromator using the laser lines at 632.8, 980.1, 1064.0, 1310.2 and 1550.8 nm. By using the second order of some of these wavelengths, we obtain 9 calibration points, extending up to 2128.0 nm with a 4 nm uncertainty. Appropriate low pass filters were inserted to avoid crosstalk from higher diffraction orders.

We measured the photon count rate (PCR) as a function of bias current and photon energy, integrating for 10 s at each point; see Fig. 2. We measured the system dark count rate (DCR) and subtracted it from our measurements. In order to compare various wavelengths, we normalise our data to a count rate value situated just below the critical current, i.e., in the plateau region where the efficiency is saturated.

To reconstruct faithfully the curves, one must pay attention to the pulse discrimination electronics. Indeed, a problem can arise when the detector operates at very low bias currents, i.e., at currents for which the amplitude of the

detection pulses is marginally higher than the amplitude of the noise of the amplifying chain and of the discriminator level. The consequence is that the shape of the PCR curve can be affected. We avoid this problem by operating only at those currents and discriminator levels, where the shape of the curves is independent of the discriminator level. See supplementary material for details.

Fig. 3 shows the energy-current relation for our MoSi detector. For each wavelength, we plot the amount of bias current I_b^η required to achieve a certain fraction η of the saturated detection efficiency (which we normalised to one in Fig. 2). Our setup allows us to measure from 0.6 eV to more than 1.6 eV in the single-photon absorption regime. We plot this relation for $\eta = 50\%$ and $\eta = 1\%$ at 0.8 K and 1.5 K, respectively. We find that the relation between bias current and photon energy is nonlinear throughout this entire measurement range for both temperatures and for both η values.

The long plateau and the broad response of our detector allow us to carefully characterise the full shape of the normalised PCR curves and compare them with the models in the literature. The curves have a transition region where the detection efficiency increases, followed by a plateau region. One theory attributes the shape of the transition region to Fano fluctuations, which are the result of the statistical nature of the quasiparticle creation process.[30,31] Since only a finite fraction of the incoming photon energy ends up in the quasiparticle bath, the number of quasiparticles generated by a photon of energy E fluctuates as $\Delta N = \sqrt{FE/\epsilon}$, where F is the Fano factor and ϵ is the energy of a single quasiparticle. These fluctuations have recently been analysed in the context of a model of quasiparticle recombination.[32] In this model, the transition region occurs because for some currents the photon only occasionally produces enough quasiparticles to trigger a detection. This results in a predicted sigmoidal shape (error function) for the PCR curve with a width that is set by the microscopic details of the down-conversion process.[33]
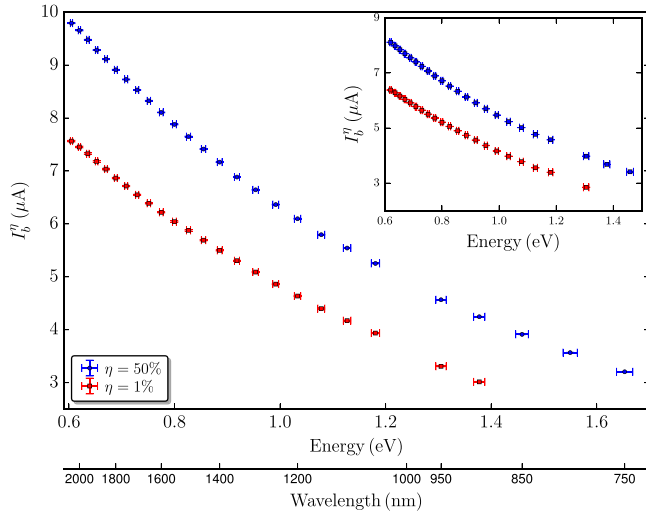
FIG. 3. Energy-current relation for two different normalised probabilities. The threshold current $I_b^{1\%}$ (red squares) and $I_b^{50\%}$ (blue points) are plotted as a function of the photon energy and corresponding wavelength at 0.8 K. Inset: Energy-current relation at 1.5 K.
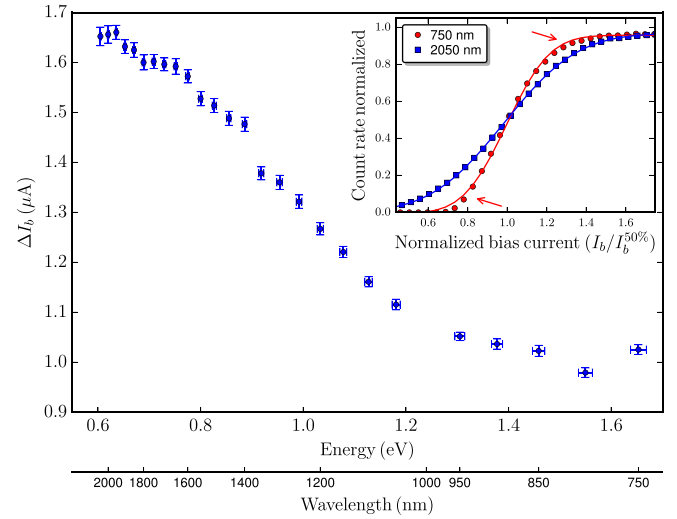

FIG. 4. Transition width defined as $\Delta I_b = I_b^{80\%} - I_b^{20\%}$ obtained from Fig. 2 as a function of the incident photon energy. Inset: photon count rate curve for 750 nm and 2050 nm as a function of the normalised bias current. The solid lines represent the error function fit (see text). The red arrows indicate the two inflection points where the data are not well described by the error function.

To check whether the Fano fluctuation theory agrees with our measurements, in Fig. 2, we fit the experimental data with an error function $R(I_b) = \text{erf}[(I_b - I_b^{50\%})/\sigma\sqrt{2}]$, where σ quantifies the width of the transition. As can be seen, at low photon energies, the fit agrees very well with the data. However, at high energies, the shape of the curves starts to deviate from the $R(I_b)$ fits. The inset in Fig. 4 shows the highest and lowest energy scans, which are overlapped to facilitate comparison. This discrepancy is statistically significant: the difference in the reduced χ^2, which quantifies the quality of the fit, is over two orders of magnitude between the lowest and highest photon energies. See supplementary material for details.

From Fig. 2, it is clear that the transition becomes narrower as the photon energy is increased. Figure 4 shows the width of the transition as a function of photon energy, defined as $\Delta I_b = I_b^{80\%} - I_b^{20\%}$. While this effect is observed in the previous studies,[18,22] we believe we present here its first quantitative description. The interpretation of this effect is still an open problem. It could originate both from Fano fluctuations[32] and position-dependent effects.[34]

The error function fit that we observe for low photon energies is indicative of Fano fluctuations. However, deviations from this shape at high energies suggest that this may not be the whole story. A possible explanation could come in the form of an additional model that predicts position dependent effects in the nanowire. In this model, different parts of the cross section of the superconducting nanowire become photodetecting at different bias currents, due to an intrinsic position dependence in the fundamental detection mechanism.[27,35] In such a model, different points in the cross-section of the wire have different energy-current relations. Consequently, this gives rise to additional broadening of the transition (in addition to the Fano fluctuations), where the width of the transition is given by $\Delta I_b = I_{\min}(E) - I_{\max}(E)$, where $I_{\min}$ and $I_{\max}$ are the threshold currents at the most efficient point (edge) and the least efficient point (middle) along the cross-section of the wire, respectively. For such a

model, one expects the width of the transition to increase with higher photon energies,[27,36] which could explain why the error function fit is not as good at higher photon energies. Moreover, due to the sharpening of the error-function transition (Fig. 4) at higher photon energies, one would expect any additional effects to be more visible, even if the position dependence effect is weakly dependent on photon energy.

We note that due to the transition width energy dependence shown in Fig. 4, the choice for η affects the shape of energy-current relation. It is therefore interesting to consider different values. The $\eta = 50\%$ value seems like a good choice in the context of the Fano fluctuations model because it corresponds to the inflexion point of the error functions used to fit the PCR curves. The $\eta = 1\%$ relation is also interesting to make a comparison with measurements based on QDT, since both are probing the energy-current relation in the rising part of the PCR curves, far below the saturation of the detection efficiency. The choice of $\eta = 1\%$ makes the energy-current relation appears closer to linear, but it remains clearly nonlinear nonetheless. We stress that the appropriate choice for η to study the physical meaning of the energy-current relation depends on the model under consideration. Comparisons between different experimental results can, however, be made in a model-independent fashion when a plateau can be clearly identified.

The nonlinear relation in MoSi is surprising in the light of previous experiments. For 220 nm-wide NbN SNSPDs made from nanobridges, and also with nanodetectors and meanders, the energy-current relation was found to be linear in the range of 0.75–8.26 eV using the quantum detector tomography (QDT).[24] A result consistent with this was found for TaN detectors[37] and for a series of NbN meanders of varying widths.[38] Nevertheless, a nonlinear behaviour for NbN meanders probed with a filtered black body light source was later observed in the 0.5–2.75 eV range[28] by using the two probability thresholds $\eta = 50\%$ and 90% of the normalised PCR. For the amorphous materials, the evidence is scarcer: a

previous study with WSi meanders found a linear relation at low energies and a single point deviating from this trend at 1.8 eV.[22] Recently, the measurements on 220 nm-wide WSi SNSPDs nanobridges[39] using QDT have shown a linear behaviour from 0.85 to 2.5 eV, but with a slight deviation from the linear behaviour between 0.75 and 0.85 eV. Reviewing this seemingly contradictory evidence, no obvious distinction between the two groups of results presents itself: neither wire width, nor device geometry, nor measurement method, nor the crystallinity of the material. While our results add additional data, the question of the detection mechanism remains an open problem. Interestingly, some recent theoretical works are predicting nonlinear energy-current relations,[23,28,32,34] but a direct comparison between these theories and our results will require more work.

In conclusion, we investigated the detection mechanism in MoSi superconductor nanowire single-photon detectors by measuring the PCR as a function of photon energy and bias current. We found a nonlinear energy-current relation in contrast to some observations on other materials, such as NbN and WSi, indicating that a model of the detection mechanism which only considers quasiparticle diffusion is incompatible with our observations. We also studied the full shape of the detection probability curve and found indications for the role of both Fano fluctuations and position-dependent effects.

See supplementary material for the complete description of the discrimination settings and χ^2 computation.

[1]G. N. Gol'tsman, O. Okunev, G. Chulkova, A. Lipatov, A. Semenov, K. Smirnov, B. Voronov, A. Dzardanov, C. Williams, and R. Sobolewski, Appl. Phys. Lett. **79**, 705 (2001).

[2]R. H. Hadfield, Nat. Photonics **3**, 696 (2009).

[3]H. Takesue, S. W. Nam, Q. Zhang, R. H. Hadfield, T. Honjo, K. Tamaki, and Y. Yamamoto, Nat. Photonics **1**, 343 (2007).

[4]F. Bussières, C. Clausen, A. Tiranov, B. Korzh, V. B. Verma, S. W. Nam, F. Marsili, A. Ferrier, P. Goldner, H. Herrmann, C. Silberhorn, W. Sohler, M. Afzelius, and N. Gisin, Nat. Photonics **8**, 775 (2014).

[5]L. K. Shalm, E. Meyer-Scott, B. G. Christensen, P. Bierhorst, M. A. Wayne, M. J. Stevens, T. Gerrits, S. Glancy, D. R. Hamel, M. S. Allman, K. J. Coakley, S. D. Dyer, C. Hodge, A. E. Lita, V. B. Verma, C. Lambrocco, E. Tortorici, A. L. Migdall, Y. Zhang, D. R. Kumor, W. H. Farr, F. Marsili, M. D. Shaw, J. A. Stern, C. Abellán, W. Amaya, V. Pruneri, T. Jennewein, M. W. Mitchell, P. G. Kwiat, J. C. Bienfang, R. P. Mirin, E. Knill, and S. W. Nam, Phys. Rev. Lett. **115**, 250402 (2015).

[6]M. Shaw, K. Birnbaum, M. Cheng, M. Srinivasan, K. Quirk, J. Kovalik, A. Biswas, A. D. Beyer, F. Marsili, V. Verma, R. P. Mirin, S. W. Nam, J. A. Stern, and W. H. Farr, in *CLEO: 2014* (Optical Society of America, 2014), p. SM4J.2.

[7]J. P. Sprengers, A. Gaggero, D. Sahin, S. Jahanmirinejad, G. Frucci, F. Mattioli, R. Leoni, J. Beetz, M. Lermer, M. Kamp, S. Höfling, R. Sanjines, and A. Fiore, Appl. Phys. Lett. **99**, 181110 (2011).

[8]P. Rath, O. Kahl, S. Ferrari, F. Sproll, G. Lewes-Malandrakis, D. Brink, K. Ilin, M. Siegel, C. Nebel, and W. Pernice, Light: Sci. Appl. **4**, e338 (2015).

[9]A. McCarthy, N. J. Krichel, N. R. Gemmell, X. Ren, M. G. Tanner, S. N. Dorenbos, V. Zwiller, R. H. Hadfield, and G. S. Buller, Opt. Express **21**, 8904 (2013).

[10]J. Zhang, N. Boiadjieva, G. Chulkova, H. Deslandes, G. N. Gol'tsman, A. Korneev, P. Kouminov, M. Leibowitz, W. Lo, R. Malinsky, O. Okunev, A. Pearlman, W. Slysz, K. Smirnov, C. Tsao, A. Verevkin, B. Voronov, K. Wilsher, and R. Sobolewski, Electron. Lett. **39**, 1086 (2003).

[11]M. G. Tanner, S. D. Dyer, B. Baek, R. H. Hadfield, and S. W. Nam, Appl. Phys. Lett. **99**, 201110 (2011).

[12]F. Marsili, V. B. Verma, J. A. Stern, S. Harrington, A. E. Lita, T. Gerrits, I. Vayshenker, B. Baek, M. D. Shaw, R. P. Mirin, and S. W. Nam, Nat. Photonics **7**, 210 (2013).

[13]Y. P. Korneeva, M. Y. Mikhailov, Y. P. Pershin, N. N. Manova, A. V. Divochiy, Y. B. Vakhtomin, A. A. Korneev, K. V. Smirnov, A. G. Sivakov, A. Y. Devizenko, and G. N. Goltsman, Supercond. Sci. Technol. **27**, 095012 (2014).

[14]V. B. Verma, B. Korzh, F. Bussières, R. D. Horansky, S. D. Dyer, A. E. Lita, I. Vayshenker, F. Marsili, M. D. Shaw, H. Zbinden, R. P. Mirin, and S. W. Nam, Opt. Express **23**, 33792 (2015).

[15]V. B. Verma, A. E. Lita, M. R. Vissers, F. Marsili, D. P. Pappas, R. P. Mirin, and S. W. Nam, Appl. Phys. Lett. **105**, 022602 (2014).

[16]M. S. Allman, V. B. Verma, M. Stevens, T. Gerrits, R. D. Horansky, A. E. Lita, F. Marsili, A. Beyer, M. D. Shaw, D. Kumor, R. Mirin, and S. W. Nam, Appl. Phys. Lett. **106**, 192601 (2015).

[17]S. N. Dorenbos, E. M. Reiger, U. Perinetti, V. Zwiller, T. Zijlstra, and T. M. Klapwijk, Appl. Phys. Lett. **93**, 131101 (2008).

[18]A. Engel, A. Aeschbacher, K. Inderbitzin, A. Schilling, K. Il'in, M. Hofherr, M. Siegel, A. Semenov, and H.-W. Hübers, Appl. Phys. Lett. **100**, 062601 (2012).

[19]J. Li, R. A. Kirkwood, L. J. Baker, D. Bosworth, K. Erotokritou, A. Banerjee, R. M. Heath, C. M. Natarajan, Z. H. Barber, M. Sorel, and R. H. Hadfield, Opt. Express **24**, 13931 (2016).

[20]E. E. Wollman, V. Verma, R. M. Briggs, A. D. Beyer, R. Mirin, S. W. Nam, F. Marsili, and M. D. Shaw, in *Conference on Lasers and Electro-Optics* (Optical Society of America, 2016), p. FW4C.4.

[21]D. Slichter, V. Verma, D. Leibfried, R. Mirin, S. Nam, and D. Wineland, preprint arXiv:1611.09949 (2016).

[22]B. Baek, A. E. Lita, V. Verma, and S. W. Nam, Appl. Phys. Lett. **98**, 251105 (2011).

[23]A. Engel, J. J. Renema, K. Il'in, and A. Semenov, Supercond. Sci. Technol. **28**, 114003 (2015).

[24]J. J. Renema, R. Gaudio, Q. Wang, Z. Zhou, A. Gaggero, F. Mattioli, R. Leoni, D. Sahin, M. J. A. de Dood, A. Fiore, and M. P. van Exter, Phys. Rev. Lett. **112**, 117604 (2014).

[25]M. K. Akhlaghi, A. H. Majedi, and J. S. Lundeen, Opt. Express **19**, 21305 (2011).

[26]A. Semenov, A. Engel, H. W. Hübers, K. Il'in, and M. Siegel, Eur. Phys. J. B **47**, 495 (2005).

[27]J. J. Renema, Q. Wang, R. Gaudio, I. Komen, K. op't Hoog, D. Sahin, A. Schilling, M. P. van Exter, A. Fiore, A. Engel, and M. J. A. de Dood, Nano Lett. **15**, 4541 (2015).

[28]D. Y. Vodolazov, Y. P. Korneeva, A. V. Semenov, A. A. Korneev, and G. N. Goltsman, Phys. Rev. B **92**, 104503 (2015).

[29]A. J. Miller, A. E. Lita, B. Calkins, I. Vayshenker, S. M. Gruber, and S. W. Nam, Opt. Express **19**, 9102 (2011).

[30]U. Fano, Phys. Rev. **72**, 26 (1947).

[31]A. G. Kozorezov, J. K. Wigmore, D. Martin, P. Verhoeve, and A. Peacock, J. Low Temp. Phys. **151**, 51 (2008).

[32]A. G. Kozorezov, C. Lambert, F. Marsili, M. J. Stevens, V. B. Verma, J. A. Stern, R. Horansky, S. Dyer, S. Duff, D. P. Pappas, A. Lita, M. D. Shaw, R. P. Mirin, and S. W. Nam, Phys. Rev. B **92**, 064504 (2015).

[33]A. Kozorezov, C. Lambert, F. Marsili, M. Stevens, V. Verma, J. Stern, R. Horansky, S. Dyer, M. Shaw, R. Mirin, and S. Nam, in Single-Photon Workshop, Geneva Switzerland (2015).

[34]D. Y. Vodolazov, preprints arXiv:1611.06060 (2016).

[35]D. Y. Vodolazov, Phys. Rev. B **90**, 054515 (2014).

[36]J. Renema, "The physics of nanowire superconducting single-photon detectors," Ph.D. thesis (Leiden University, 2015).

[37]A. Engel and A. Schilling, J. Appl. Phys. **114**, 214501 (2013).

[38]R. Lusche, A. Semenov, K. Ilin, M. Siegel, Y. Korneeva, A. Trifonov, A. Korneev, G. Goltsman, D. Vodolazov, and H.-W. Hübers, J. Appl. Phys. **116**, 043906 (2014).

[39]R. Gaudio, J. J. Renema, Z. Zhou, V. B. Verma, A. E. Lita, J. Shainline, M. J. Stevens, R. P. Mirin, S. W. Nam, M. P. van Exter, M. J. A. de Dood, and A. Fiore, Appl. Phys. Lett. **109**, 031101 (2016).